Developmental Cell, Volume *41*

Supplemental Information

An Orchestrated Intron Retention Program in Meiosis Controls Timely Usage of Transcripts during Germ Cell Differentiation

Chiara Naro, Ariane Jolly, Sara Di Persio, Pamela Bielli, Niclas Setterblad, Antonio J. Alberdi, Elena Vicini, Raffaele Geremia, Pierre De la Grange, and Claudio Sette

Inventory of Supplemental Information

Supplemental Figures

Supplemental Tables

Supplemental Figures

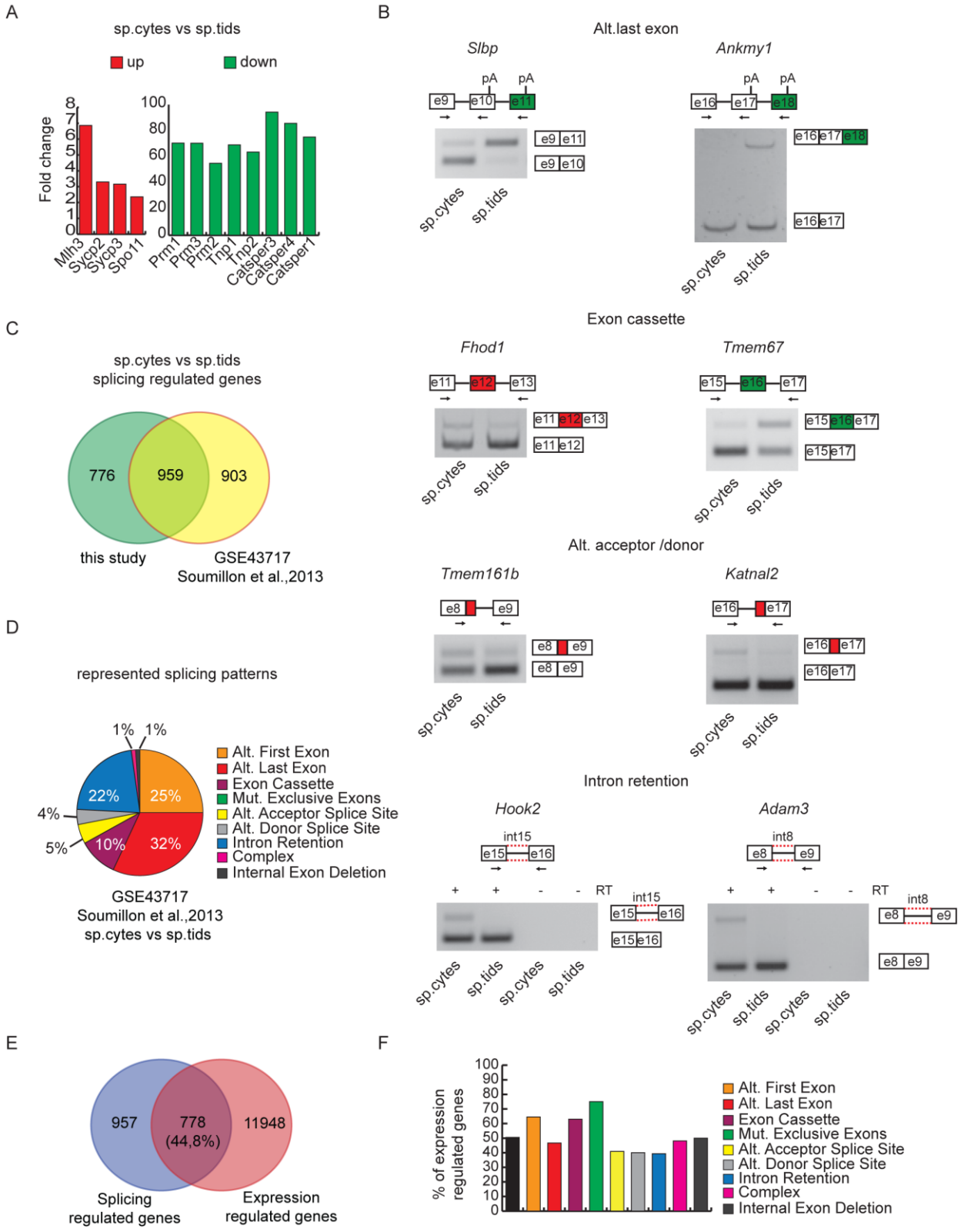

Figure S1. Analysis and validation of RNA-seq results, related to Figure 1. A) Bar graphs showing intensity of the expression fold-change between sp.cytes and sp.tids resulting from the RNA-seq analysis for indicated representative genes with known regulated expression during trans-

meiotic differentiation. B) Representative images of RT-PCR analyses for indicated AS events differentially regulated between sp.cytes and sp.tids. Red and green boxes indicate respectively up- and down-regulated events in sp.cytes compared to sp.tids. Schematic representation for each splicing event analyzed is depicted above the representative agarose or acrylamide gel. Black arrows in the scheme indicate primers used for the PCR analysis. C) Venn diagram showing overlap between groups of splicing-regulated genes between sp.cytes and sp.tids identified in this study (green circle) and by the analysis of datasets from the same cell types originated in a previous study (GSE43717, Soumillon et al., 2013) Overlap is highly significant: p-value=0; modified Fisher's test. D) Pie chart representing distribution among different splicing patterns of the regulated splicing events between sp.cytes and sp.tids revealed by analysis of GSE43717 datasets (Soumillon et al., 2013). E) Venn diagram showing percentage of overlap between group of expression- and splicing-regulated genes in sp.cytes vs sp.tids. F) Bar graph representing percentage of expression-regulated genes among the splicing regulated genes within each different splicing pattern.

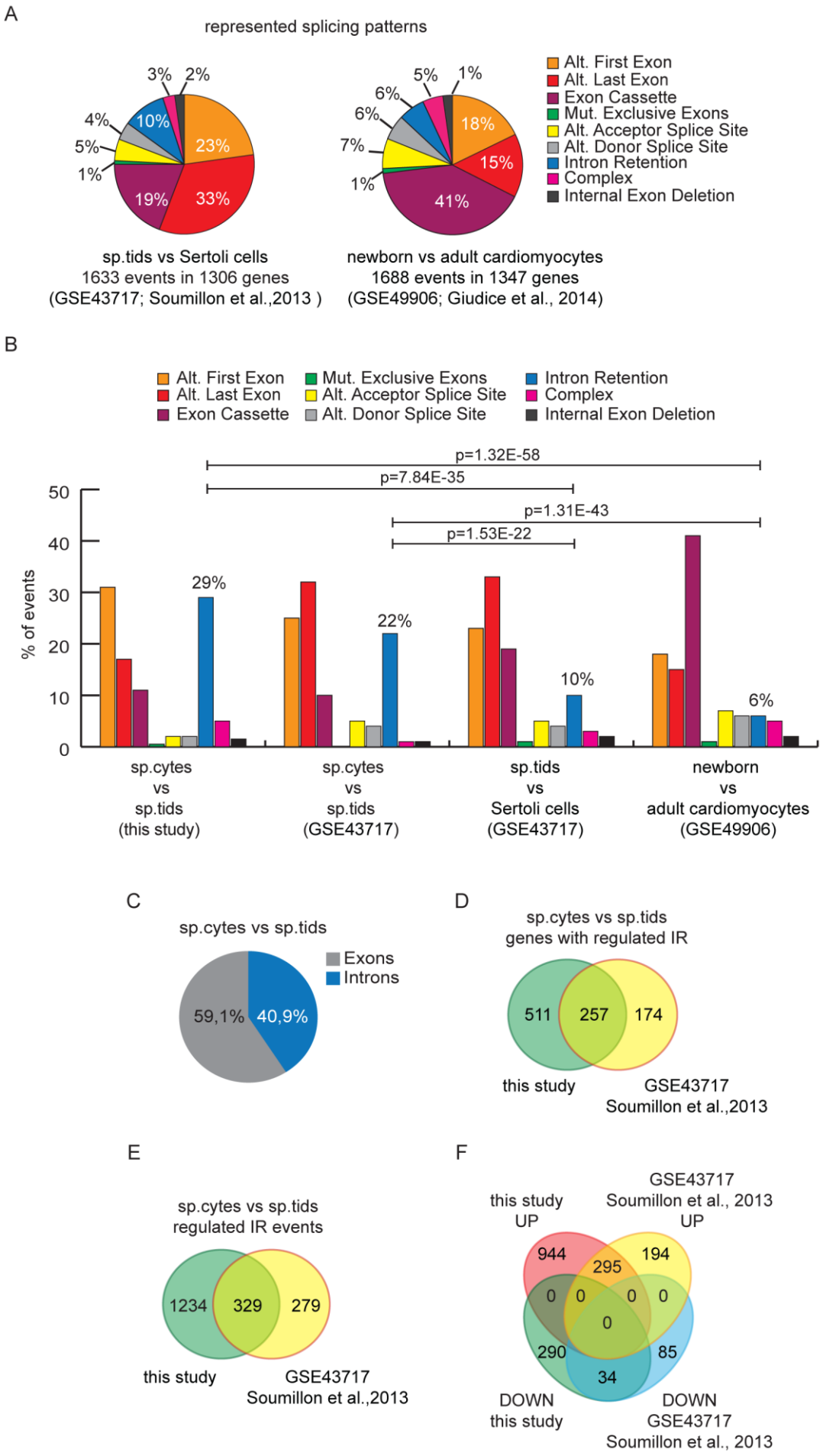
A
represented splicing patterns
3%
2%
4%
10%
5%
23%
1%
19%
33%
5%
1%
6%
6%
18%
7%
15%
1%
41%
Alt. First Exon
Alt. Last Exon
Exon Cassette
Mut. Exclusive Exons
Alt. Acceptor Splice Site
Alt. Donor Splice Site
Intron Retention
Complex
Internal Exon Deletion
sp.tids vs Sertoli cells
1633 events in 1306 genes
(GSE43717; Soumillon et al.,2013)
newborn vs adult cardiomyocytes
1688 events in 1347 genes
(GSE49906; Giudice et al., 2014)
B
Alt. First Exon
Alt. Last Exon
Exon Cassette
Mut. Exclusive Exons
Alt. Acceptor Splice Site
Alt. Donor Splice Site
Intron Retention
Complex
Internal Exon Deletion
p=1.32E-58
p=7.84E-35
p=1.31E-43
p=1.53E-22
% of events
50
40
30
20
10
0
29%
22%
10%
6%
sp.cytes vs sp.tids (this study)
sp.cytes vs sp.tids (GSE43717)
sp.tids vs Sertoli cells (GSE43717)
newborn vs adult cardiomyocytes (GSE49906)
C
sp.cytes vs sp.tids
Exons
Introns
59,1%
40,9%
D
sp.cytes vs sp.tids
genes with regulated IR
511
257
174
this study
GSE43717
Soumillon et al.,2013
E
sp.cytes vs sp.tids
regulated IR events
1234
329
279
this study
GSE43717
Soumillon et al.,2013
F
this study
UP
GSE43717
Soumillon et al., 2013
UP
944
295
194
0
0
0
0
0
290
85
34
DOWN
this study
DOWN
GSE43717
Soumillon et al., 2013

Figure S2. Intron retention features transcriptome of meiotic male germ cells, related to Figure 2. A) Pie charts representing distribution among different splicing patterns of the regulated splicing events between sp.tids and somatic Sertoli cells (left chart) and between newborn and adult cardiomyocytes (right chart) revealed by analysis of previously published RNA-seq datasets (GSE43717, Soumillon et al., 2013; GSE49906, Giudice et al., 2014). B) Analysis of RNA-seq data from both our and previously published studies revealed a significant enrichment of IR events (blue bars) in the comparison between sp. cytes and sp.tids germ cells respect to the other indicated developing/differentiation systems (p-values of Chi2 test are shown). C) Pie chart depicting proportions of exonic and intronic events among the regulated splicing events in sp.cytes compared to sp.tids. D, E) Venn diagrams showing overlap between IR genes (D) and regulated IR events (E) in sp.cytes compared to sp.tids identified in this study (green circle) and by analysis of a previous dataset (Soumillon et al., 2013). P-value = 6.97E-164 for overlap in D, p-value = 0 for overlap in E according to modified Fisher's test. F) Venn diagram showing overlap in the direction of the regulation of the IR events regulated between sp.cytes and sp.tids in this study and in analysis of Soumillon et al., 2013 dataset. P-value = 0 according to modified Fisher's test.

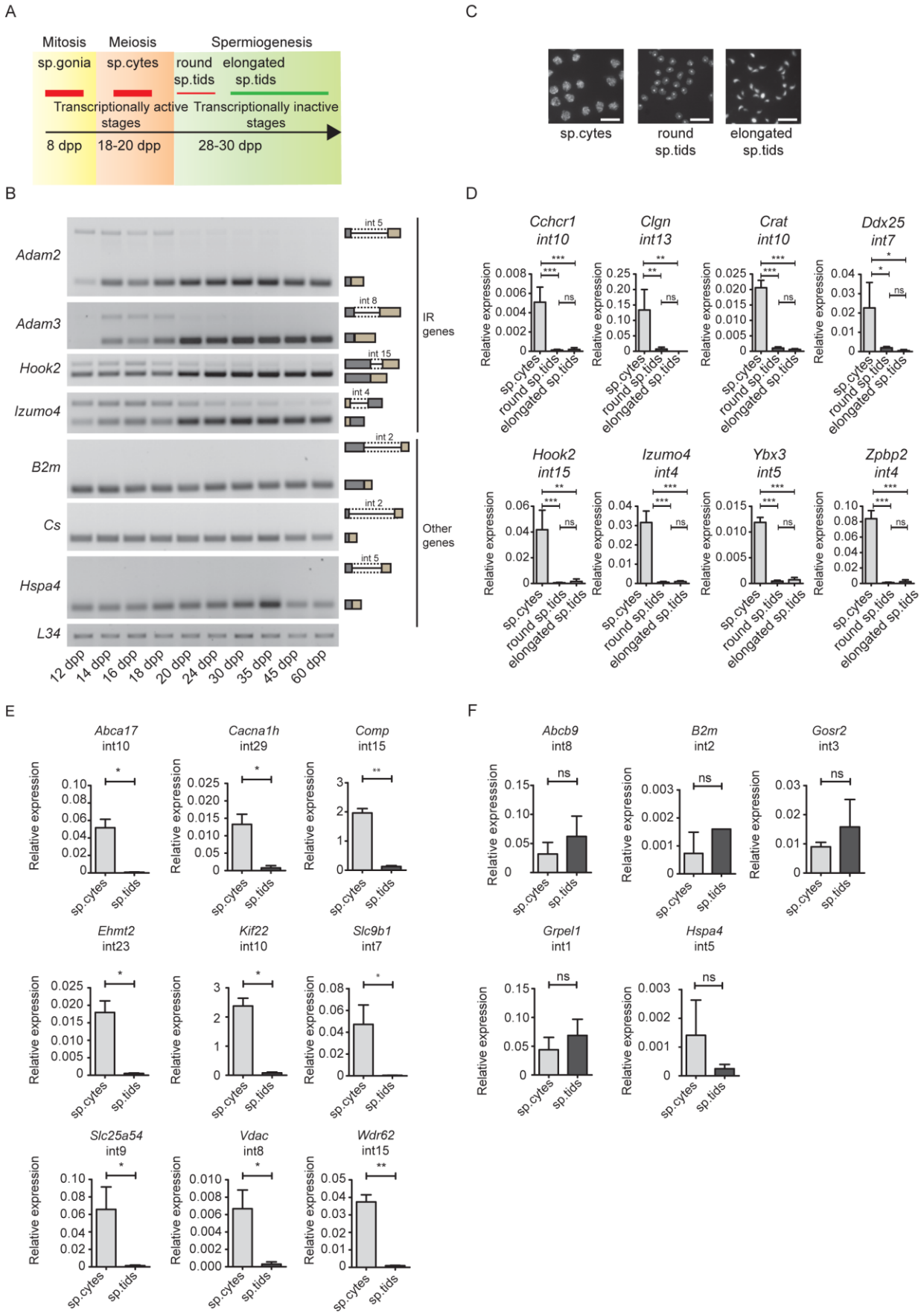
A
Mitosis
Meiosis
Spermiogenesis
sp.gonia
sp.cytes
round sp.tids
elongated sp.tids
Transcriptionally active stages
Transcriptionally inactive stages
8 dpp
18-20 dpp
28-30 dpp
C
sp.cytes
round sp.tids
elongated sp.tids
B
Adam2
Adam3
Hook2
Izumo4
B2m
Cs
Hspa4
L34
int 5
int 8
int 15
int 4
int 2
int 2
int 5
IR genes
Other genes
12 dpp
14 dpp
16 dpp
18 dpp
20 dpp
24 dpp
30 dpp
35 dpp
45 dpp
60 dpp
D
Cchcr1 int10
Clgn int13
Crat int10
Ddx25 int7
Hook2 int15
Izumo4 int4
Ybx3 int5
Zpbp2 int4
Relative expression
sp.cytes
round sp.tids
elongated sp.tids
E
Abca17 int10
Cacna1h int29
Comp int15
Ehmt2 int23
Kif22 int10
Slc9b1 int7
Slc25a54 int9
Vdac int8
Wdr62 int15
Relative expression
sp.cytes
sp.tids
F
Abcb9 int8
B2m int2
Gosr2 int3
Grpel1 int1
Hspa4 int5
Relative expression
sp.cytes
sp.tids
ns

Figure S3. Validation of intron retention events occurring in meiotic spermatocytes, related to Figure 2. A) Schematic representation of the timeline of murine spermatogenesis, its key phases and their transcriptional activity. B) Representative images of RT-PCR analyses for indicated IR-regulated and properly spliced genes in mouse testes from animals of indicated age during the first wave of spermatogenesis. Black arrows in the scheme indicate primers used for the PCR analysis. C) Representative images of Hoechst nuclear staining of purified cellular populations of meiotic pachytene spermatocytes (sp.cytes, left panel), early-stage round (middle panel) and late-stage elongated spermatids (sp.tids, right panel; scale bar 25 μm). D) Bar graphs showing results of qPCR analyses for the expression of indicated introns relative to spliced product of their flanking exons in sp.cytes, round and elongated sp.tids (mean ±SD, n=4, *p-value≤0.05; **p-value≤0.01; ***p-value≤0.001; ns=not significant - one-way ANOVA test). E,F) Bar graphs showing results of qPCR analyses for the expression of indicated introns relative to spliced product of their flanking exons in sp.cytes and round sp.tids (mean ±SD, n=3, *p-value≤0.05; **p-value≤0.01; according to two-tailed t-test; ns=not significant). Properly spliced introns of the *Abcb9, B2m, Gosr2, Grpel1*, and *Hspa4*genes were evaluated as control (F).

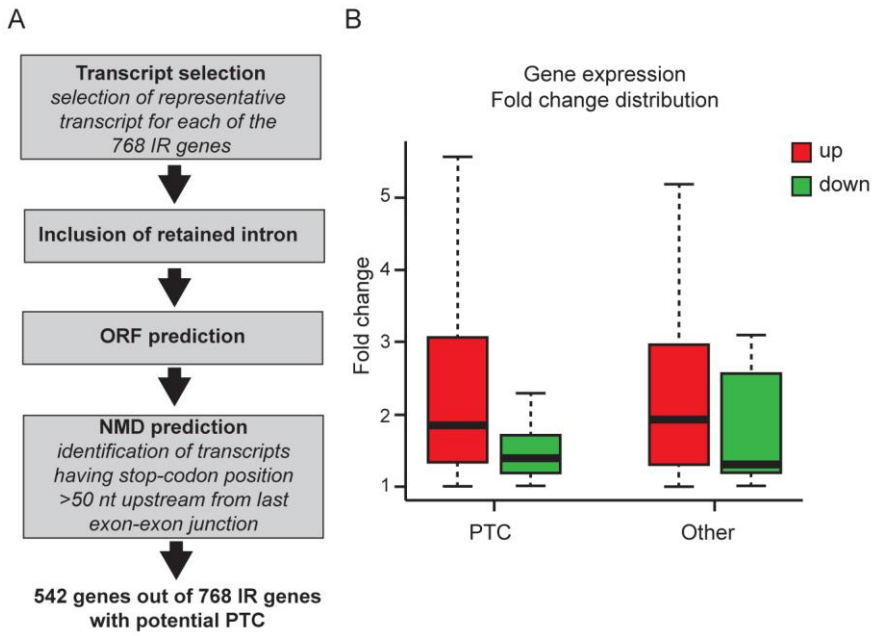

Figure S4. Meiotic IRTs are unlikely substrates for the NMD degradation pathway, related to Figure 3. A) Schematic representation of the workflow used for the identification of the IR events leading to PTC generation. B) Box plot showing distribution of fold change between spermatocytes and spermatids for genes with IR predicted (PTC) or not (other) to have PTC. No significant difference in term of expression regulation was observed between the two groups (p-value = 8.84E-1, modified Fisher's test).

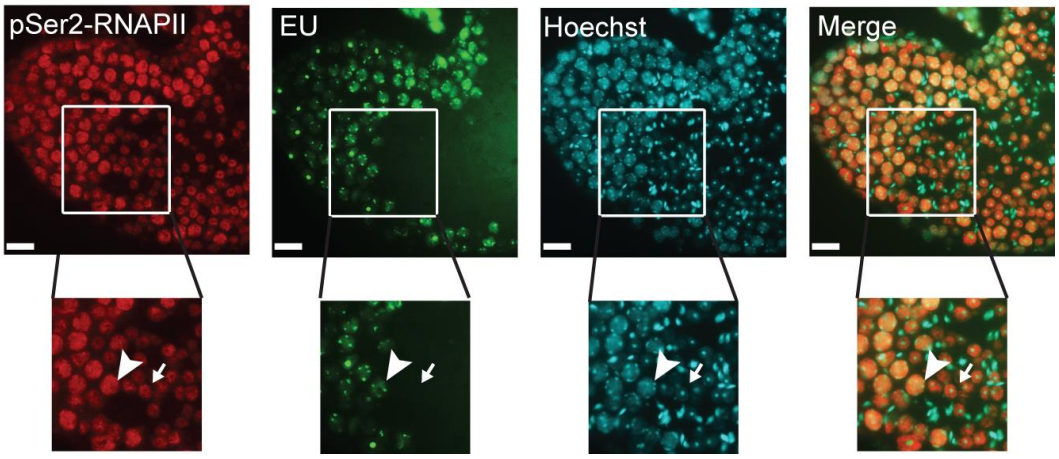

Figure S5. pSer2-RNAP II and EU-labelled RNAs mark meiotic male germ cells, related to Figure 5. pSer2-RNAPII using H5 antibody and EU-staining with Alexa488-azide of cross-sections of seminiferous tubules from adult mice cultured for 2 h 30 min in presence of EU 1mM. Hoechst staining was used to identify nuclear morphology (scale bar 25 µm). Insets show magnification of meiotic spermatocytes (arrow head) and post-meiotic round spermatids (arrow).

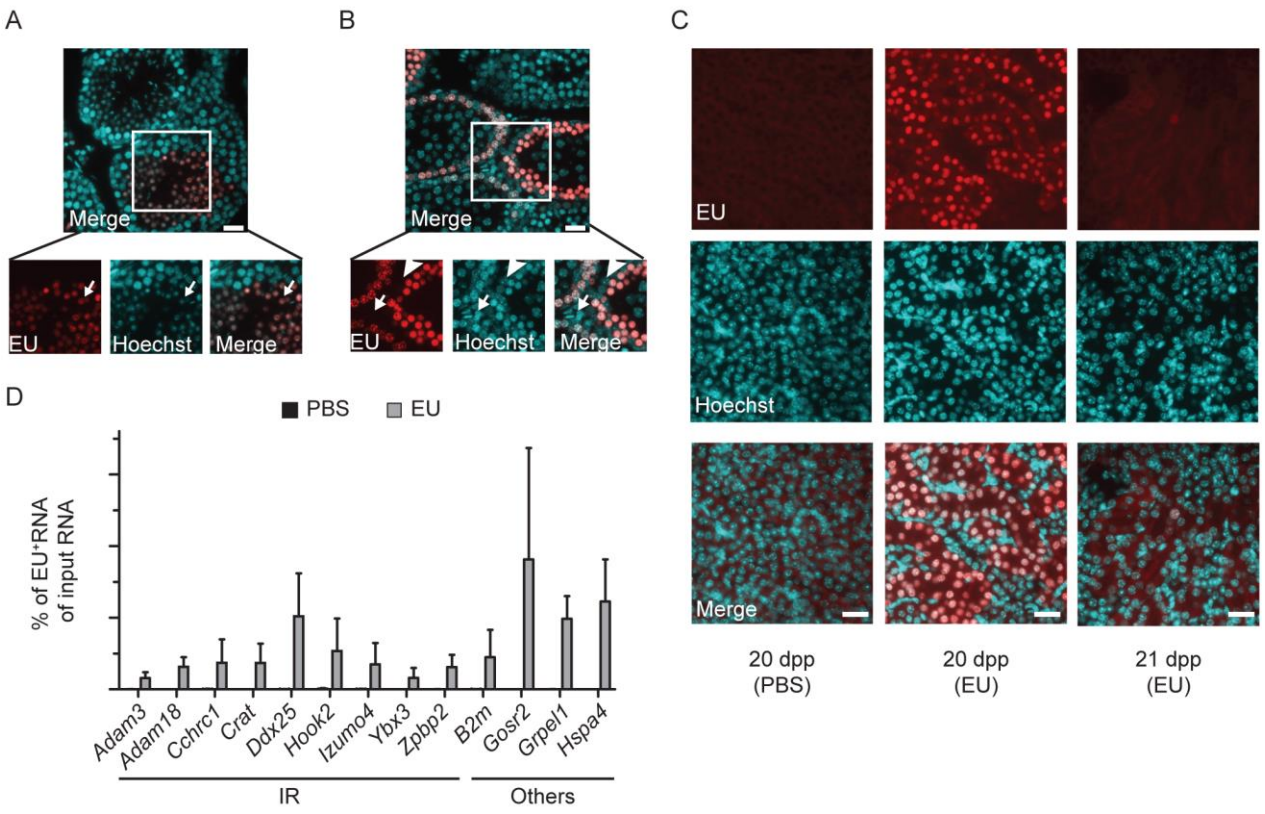

Figure S6. EU labels RNA also in kidney and with similar intensity between properly spliced and intron retaining transcripts, related to Figure 6. A,B) EU-staining with Alexa594-azide of testes paraffin-embedded cross-sections from EU- injected mice harvested at 29 dpp (A), 21 dpp (B). Hoechst nuclear staining was performed to identify nuclear morphology (scale bar 25 µm). Insets show magnification images of post-meiotic round spermatids (arrow in A), somatic Sertoli (arrow head in B) and interstitial cells (arrow in B). C) EU-staining with Alexa594-azide of kidney paraffin-embedded cross-sections of EU- and PBS (as control) injected mice, analyzed at indicated time points. Hoechst was used for nuclei staining (scale bar 25 µm). D) Bar graph showing the percentage of EU-labeled RNA pulled-down from total RNA for indicated transcripts at indicated time points estimated by qPCR analysis (mean ±SD, n=3).

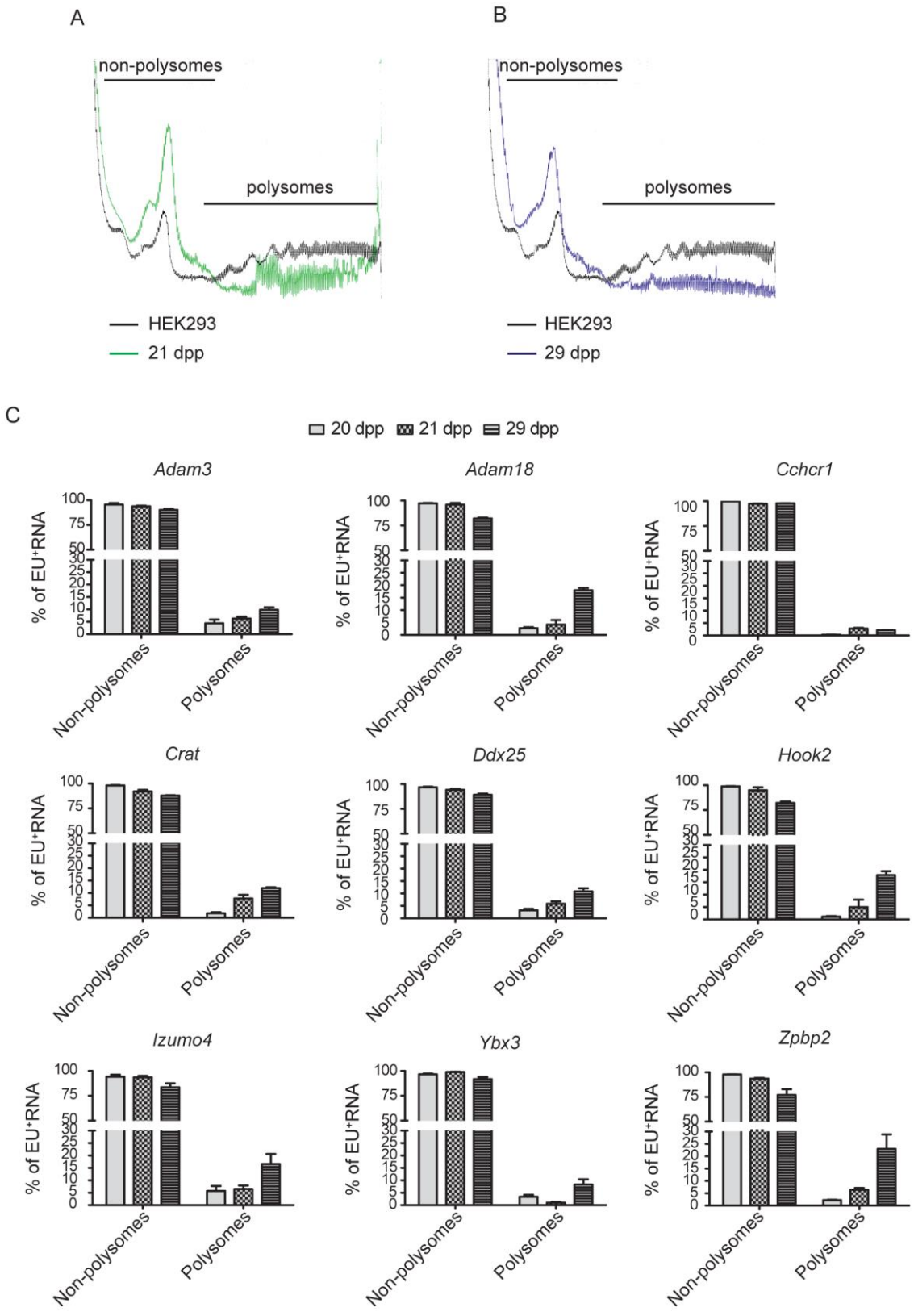

Figure S7. Related to Figure 7. RNP-polysome fractionation profile of whole testes A,B) Absorbance profile (OD = 260 nm) of sucrose gradient sedimentation of extracts from mitotic HEK293 cells (black line) and testes of 21 (green line, A) and 29 dpp mice (blue line, B). C) Bar

graph showing qPCR analysis for the distribution of EU-labeled RNAs pulled-down for indicated genes within the polysomal and non-polysomal fractions obtained from sucrose gradient fractionation of whole testes harvested at indicated time point after EU injection at 20 dpp (mean ±SD, n=3). Results are expressed as percentage of the total EU-labeled RNA captured in all fractions of the gradient.